Passive Pressure-Drag Control in a Plane Wake

F. F. Grinstein,* J. P. Boris,† and O. M. Griffin‡
Naval Research Laboratory, Washington, D.C. 20375

We report results of a study of the transition region of a compressible (subsonic) plane wake at moderately high Reynolds numbers, based on the numerical solution of the inviscid time-dependent flow equations. The focus is placed on the flow dynamics in the region of vortex formation and the near wake. A thin interference plate along the wake centerline, which can either be attached or detached from the bluff-body base, is used as a means for passive pressure-drag control by affecting the vortex formation process directly. The results show that the inclusion of an interference plate in the flow configuration can significantly decrease the magnitude of the base pressure coefficient by factors of up to 3, depending on the length of the plate and its separation from the base. The calculated results are in good agreement with the available experimental data and include the detached case for which little or no data exists. The observed self-sustained (global) instabilities in the present simulations were found to be intrinsic features of the flows investigated and are consistent with the local absolute/global instability picture currently favored.

Nomenclature

C_{pb} = base-pressure coefficient
h = bluff-body thickness
h' = wake thickness
K = base-pressure parameter
l = separation between interference plate and bluff-body base
M = Mach number
P = static pressure
P_{amb} = ambient static pressure
Re = $U_\infty h/\nu_{eff}$
St = shedding (Strouhal) frequency based on h and U_∞
U_∞ = inflow velocity
u' = root-mean-square streamwise velocity fluctuations
δ_s = boundary-layer thickness
θ_s = momentum thickness
ν_{eff} = effective viscosity
ρ_∞ = inflow mass density

Introduction

KNOWLEDGE of the basic character of the underlying fluid-dynamic processes in bluff-body near-wake flows is necessary to achieve control of lift and drag in many practical external flows. Recent theoretical studies using linear stability analysis have shed new light on the local absolute/convective nature of wake-flow instabilities,[1] providing a new framework for understanding the dynamics of vortex-street formation and evolution. Numerical simulations of wake flows evolving in both space and time extend these theoretical studies to practical regimes by accounting for the nonparallel nature of the flows, for global instabilities due to nonlinear and subharmonic feedback, and for effects induced by the presence of stationary bodies on the near-wake flow.

It is generally accepted that the pressure drag is due to the region of negative base pressure associated with the inward spiraling of the vorticity layer shed from the surface of the bluff body. Noting that the magnitude of the pressure drag is dependent on the strength of the vortices and on the length of the vortex formation region, it was recognized in the early studies of wake flows (e.g., Ref 2) that the drag-inducing base-pressure drop can be reduced in practice by interfering with the process of vortex formation. By modifying or suppressing the vortex formation region with interference plates, the drag of a bluff body was reduced in laboratory experiments[2-5] and in numerical simulations.[6] Only recently[5] have extensive laboratory studies of bluff-body near-wake flows with fixed separation points been reported, including the effects of a gap between the interference plate and the base of a rectangular cylinder with a separation angle of 90 deg.

In this work, we focus on the wake behind a long bluff body with a rectangular trailing edge, corresponding to the case with a separation angle of 0 deg. We report results of two-dimensional numerical simulations of the transition region of a compressible (subsonic), spatially evolving plane wake at moderate and high Reynolds numbers. The present studies of pressure-drag control and modification use a thin, friction-free, flow-aligned interference plate, which is either attached or detached from the base, to directly control the vortex formation process. The focus of this work is on the flow dynamics in the vortex formation region and the near wake. The

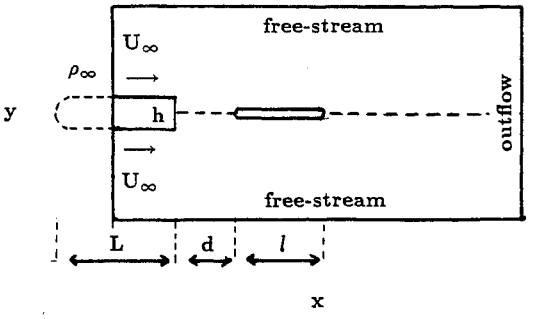

Fig. 1 Schematic flow configuration. The thin interference plate of length l begins a distance d downstream of the bluff body's trailing edge.

Presented as Paper 90-0507 at the AIAA 28th Aerospace Sciences Meeting, Reno, NV, Jan. 8-11, 1990; received May 21, 1990; revision received Nov. 13, 1990; accepted for publication Nov. 14, 1990. This paper is declared a work of the U.S. Government and is not subject to copyright protection in the United States.

*Research Physicist, Laboratory for Computational Physics and Fluid Dynamics, Code 4410. Member AIAA.

†Chief Scientist, Laboratory for Computational Physics and Fluid Dynamics, Code 4400. Member AIAA.

‡Research Mechanical Engineer, Center for Advanced Space Sensing, Laboratory for Computational Physics and Fluid Dynamics, Code 4223.1.

results effectively show the influence of passive control with interference plates on the vortex formation process in the plane wake.

Numerical Model

The basic flow configuration and boundary conditions used in the simulations are shown schematically in Fig. 1. The bluff body has a rectangular shape with height h much smaller than its streamwise and spanwise extent, and it is assumed that its D-shaped leading edge is outside of the computational domain. The streamwise length L of the body is assumed to be sufficiently short so that boundary-layer effects are minor for the fast flow regimes considered. In order to evaluate the base-pressure drag using the data base from the computations, knowledge of the pressure at the leading side of the bluff body is also required. In principle, this information is not directly available because the whole bluff body is not included in the computational domain. However, the pressure on the leading side of the body can be consistently regarded to be ambient pressure P_{amb} if the flow configuration of Fig. 1 corresponds to that of the flow about a long, blunt-based bluff body with a D shape on its leading edge.

The simulations are performed for identical laminar coflowing streams of air initially separated by the bluff body with freestream velocity U_∞ in the range $1.0\text{–}2.0 \times 10^4$ cm/s, and freestream Mach numbers in the range 0.3–0.6 at standard initial temperature and pressure conditions. A thin interference plate of length l placed along the centerline begins a distance d from the bluff-body base and is used in some of the calculations to control the base pressure by directly affecting the fluid dynamics of the vortex formation region.

The numerical model is based on the time-dependent inviscid conservation equations for mass, momentum, and energy density for an ideal gas. A passive scalar convected separately with the velocity field is used to evaluate the flow entrainment. The model uses the flux-corrected transport (FCT) algorithm with directional timestep-splitting techniques on structured grids.[7,8] FCT is an explicit, conservative, monotone, finite difference algorithm, requiring no explicit artificial viscosity for stabilization. No explicit turbulence subgrid modeling other than the natural FCT high-frequency filtering has been included. The nonlinear properties of the FCT algorithm effectively act as a minimal subgrid model by maintaining the large-scale structures without aliasing while numerically smoothing the scales with wavelengths smaller than a few computational cells. The approach has been shown to be suitable for simulating the large-scale features of high Reynolds number vorticity dynamics in transitional free shear flows (see, e.g., Refs. 9–10 and references therein). A fourth-order phase-accurate FCT algorithm is used in the calculations.

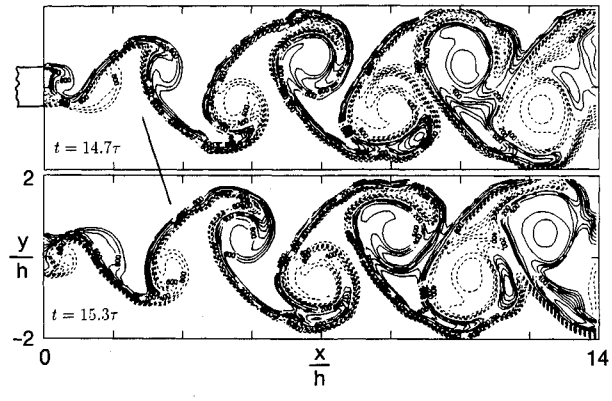

Fig. 2 Instantaneous flow visualization for $M = 0.6$ and $Re \sim 4.0 \times 10^4$. Contours of a passive mixing scalar: $\phi > 0$; dashed contours, $\phi < 0$. Time is scaled with the shedding period τ.

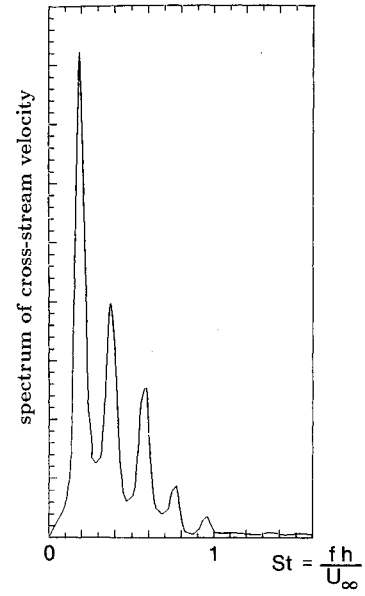

Fig. 3 Typical spectrum of transverse velocity fluctuations in the near wake for the case of Fig. 2. The vertical scale is linear.

Ideal, free-slip wall conditions are imposed on the interference plate and bluff body. Inflow and outflow boundary conditions are imposed where appropriate in the streamwise direction x, and freestream boundary conditions are imposed in the cross-stream direction y. The density and velocities are specified at the inflow guard cells. A zero-gradient condition on the pressure allows the inflow pressure to vary in response to acoustic waves generated by the fluid accelerations downstream. At the outflow, linear advection equations are imposed using the local velocity near the boundary, and the pressure is relaxed toward the specified ambient value P_{amb}. The inflow and outflow boundary conditions used in the model were developed and tested extensively in previous shear-flow simulations.[8-10] Results of specific tests in the case of the present numerical studies are discussed in the next section and will be extensively analyzed in a forthcoming report.[11]

A short inflow plenum is modeled by including a portion of the bluff body within the computational domain in the simulations. A constant uniform mass flux is effectively imposed at the inflow. The sharp edges of the initial mass-flux profile are smoothed within a few computational cells by the small residual numerical viscosity of the algorithm into a doubly inflectional wake profile. For Mach numbers $M \lesssim 0.5$, and when the gridding involves evenly spaced computational cells, an effective viscosity ν_{eff} can be defined, behaving as $\nu_{eff} \sim \mathcal{O}(\Delta r)^{1.5}$ for fixed Courant numbers, where Δr is the mesh spacing.[12] In the present work, characteristic Reynolds numbers based on U_∞, h, and ν_{eff} are in the range $10^3 \lesssim Re \lesssim 4 \times 10^4$.

The gridding is uniform in the regions where entrainment takes place. The computational cells are stretched in the cross-stream direction as the freestream boundaries in the transverse direction are approached, but are otherwise uniformly spaced. The number of computational cells varies in the range of 110–232 in the cross-stream direction and 173–600 in the streamwise direction. Stretching of the grid in the streamwise direction was also used downstream of the flow region of interest in the larger computational domains. The grid is held fixed in time. Courant numbers in the range of 0.3–0.5 are used in the numerical simulations. Studies doubling and coarsening the resolution of the mesh indicated that the convergence of calculated quantities, such as base-pressure coefficients and shedding frequencies, is better than 2%. The codes are fully vectorized for efficient processing. Typical calculations on the CRAY-YMP require about 17 μs of CPU time per time step per grid point.

Results and Discussion

Figure 2 shows the calculated evolution of the two-dimensional unforced wake visualized through contours of a passive mixing scalar ϕ defined to be of unit magnitude but of opposite signs for the two initial freestreams at the inflow. The figure shows the alternate shedding of spanwise rollers of opposite sign that give rise to the vortex street characteristic of the wake flows. Figure 3 shows a typical spectrum of transverse velocity fluctuations in the near wake for a simulated flow without interference plate for $M = 0.6$. The particular spectrum was obtained at $x = 4h$, $y = h/2$ and shows a main peak at $St = fh/U_\infty \sim 0.19$–$0.2$, corresponding to the natural vortex shedding frequency, and shows minor peaks at its harmonics. Depending on M, Re, and of the particular flow configurations, the shedding frequencies St in the simulations were found to be in the range of 0.19–0.30, in good agreement with the experimental values summarized in Table 1.

Because the inflow pressure varies in response to the acoustic events downstream, it is conceivable that a resonance could occur and thus force the flow. This is not different from the usual situation of laboratory experiments where artificial boundaries due to the finite size of the facilities and feedback effects are at some level unavoidable. Thus, an important issue addressed was the effect of the outflow boundary conditions, which specify the way in which the simulated flow conditions relax to ambient conditions, and their interaction with the inflow boundary conditions. In order to assess the effect of the boundary conditions, selected simulations were redone on much larger computational domains (see Fig. 4), including a longer inflow plenum and much larger separation between the cross-stream and streamwise boundaries. Additional studies examined the effects of grid stretching (when applicable), which is capable of producing weak (spurious) pressure-wave reflections as well as (numerically) dissipating the flow structures and waves as they exit the near-wake region of interest. The results indicated that the flow features were virtually unchanged.[11] As an example, the changes in the calculated shedding frequencies were $< 1.5\%$ for all grid sizes and stretching parameters considered.

Typical contours of spanwise vorticity Ω_z and relative static pressure difference $(P - P_{amb})/P_{amb}$ are shown in Figs. 5a and 5b, corresponding to the bottom frame of Fig. 2. The instantaneous relative pressure drops of 25–30% (at $M = 0.6$) in the cores of the newly shed spanwise rollers are responsible for a low-pressure region just downstream of the base of the body, where the pressure fluctuates as the vortices form. The net effect of the vortex formation process is the time-averaged pressure minimum observed in Fig. 6a, the main generation mechanism for the base-pressure drag.

Contours of the rms normalized streamwise velocity fluctuations $u' = (\overline{u^2} - \bar{u}^2)^{1/2}/U_\infty$ are shown in Fig. 6b, where the main peaks are associated with the vortex shedding. The minimum transverse separation between peaks in the profiles of u' at fixed streamwise locations coincides with the distance between free streamlines and is used to define the wake thickness h'.[2,3] The streamwise location where that minimum transverse separation between peaks occurs is found near that of the minimum mean pressure along the centerline of the wake (here, at $x \approx h/2$) and defines the end of the vortex formation region and the beginning of the developed vortex street.

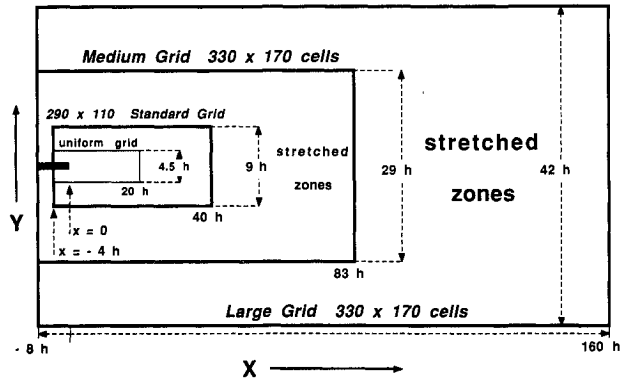

Fig. 4 Computational domains used in the numerical simulations.

Table 1 Natural vortex shedding (Strouhal) frequency for blunt-based models without interference plates

No interference plate	
Present	
$M = 0.6, L/h \gg 1, Re \sim 1.4 \times 10^4 \rightarrow 4 \times 10^4$	0.19 → 0.20
$M = 0.3, L/h \gg 1, Re \sim 1.2 \times 10^3, l = 0$	0.24
Heinemann[16]	
$M = 0.6, L/h = 20, Re = 6 \times 10^5$	0.18
$M = 0.6, L/h = 33, Re = 6 \times 10^5$	0.19
Bearman[3]	
Virtually incompressible	
$L/h = 6, Re = 1.45 \times 10^5 \rightarrow 2.45 \times 10^5$	0.24
Simmons[14]	
Virtually incompressible	
$L/h = 1.5, Re = 1.5 \times 10^4$	0.25
With interference plate	
Present simulations	
$M = 0.3, L/h \gg 1, Re \sim 1.2 \times 10^3, l = h, d = h$	0.11
$M = 0.3, L/h \gg 1, Re \sim 1.2 \times 10^3, l = h, d = 2h$	0.23
$M = 0.3, L/h \gg 1, Re \sim 1.2 \times 10^3, l = h, d = 0$	0.28
Bearman[3]	
Virtually incompressible	
$L/h = 6, Re = 1.45 \times 10^5 \rightarrow 2.45 \times 10^5$, $l = h, d = 0$	0.28 → 0.30

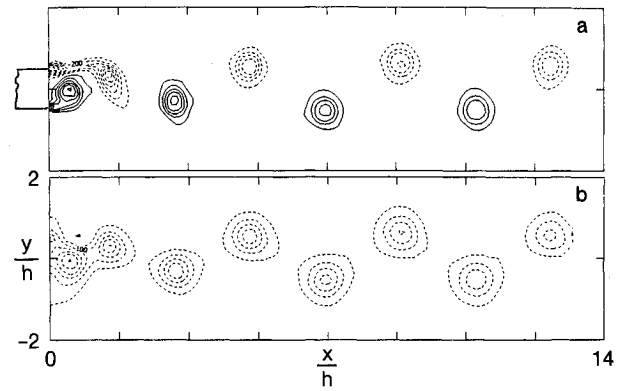

Fig. 5 Instantaneous flow visualization corresponding to the bottom frame of Fig. 2: a) contours of spanwise vorticity (solid; positive; dashed; negative); b) contours of relative static pressure difference $(P - P_{amb})/P_{amb}$.

A general similarity of near-wake flows has been established over the years.[2,3,12] In particular, this similitude becomes apparent when we plot h'/h as a function of the base-pressure parameter $K = (1 - C_{pb})^{1/2}$, where $C_{pb} = (P_b - P_{amb})/(\frac{1}{2}\rho_\infty U_\infty^2)$ is the base-pressure coefficient, for bluff bodies with various geometries and initial conditions (i.e., self-excited or forced, with or without interference plates).[13] Figure 7, which is based on Fig. 8 of Ref. 12, shows the direct relationship between bluffness (as measured by h') and pressure drag or base suction (as measured by K). Larger bluffness is associated with wider wakes and larger pressure drag. The experimental results in Fig. 7 include body shapes ranging from stationary, blunt-based D-shaped cylinders with Reynolds numbers in the range of 10^4–2.5×10^5 with aspect ratios of 6:1,[3] 1.5:1,[14] and 19:1,[15] to stationary circular cylinders at Reynolds numbers in the range of 120–2×10^5, and to wedges, flat plates, and half-cylinders normal to the incident flow. The scatter in the experimental data is due to variations in separation point variability, i.e., fixed as in the flat plate and D-section cylinders vs free for the circular cylinder,

Table 2 Legend for data in Figure 7

Symbol	Bluff-body type	Method	Investigators
●	Half cylinder (D-section)	Wind tunnel experiment	Armstrong et al.[17]
	Flat plate	Wind tunnel experiment	Armstrong et al.[17]
●	Circular cylinder	Wind tunnel experiment	Armstrong et al.[17]
○	Circular cylinder	Wind tunnel experiment	Barbi et al.[18]
◪ □ ■ ■	D-section with and without interference	Computation	Grinstein et al. (present work)
	Hydrofoil	Wind tunnel experiment	Blake et al.[15]
+	D-section cylinder	Wind tunnel experiment	Simmons[14]
▽ ▽	D-section cylinder with and without interference	Wind tunnel experiment	Bearman[3]

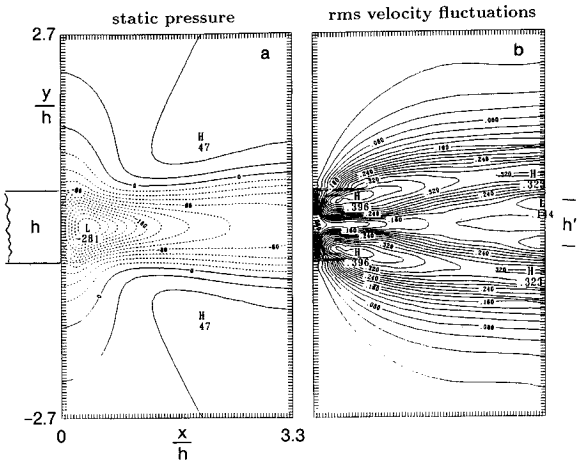

Fig. 6 Time-averaged flow quantities in the vortex formation region: a) static pressure, $(P - P_{amb})/P_{amb}(\times 10^3)$; b) normalized rms velocity fluctuations u'.

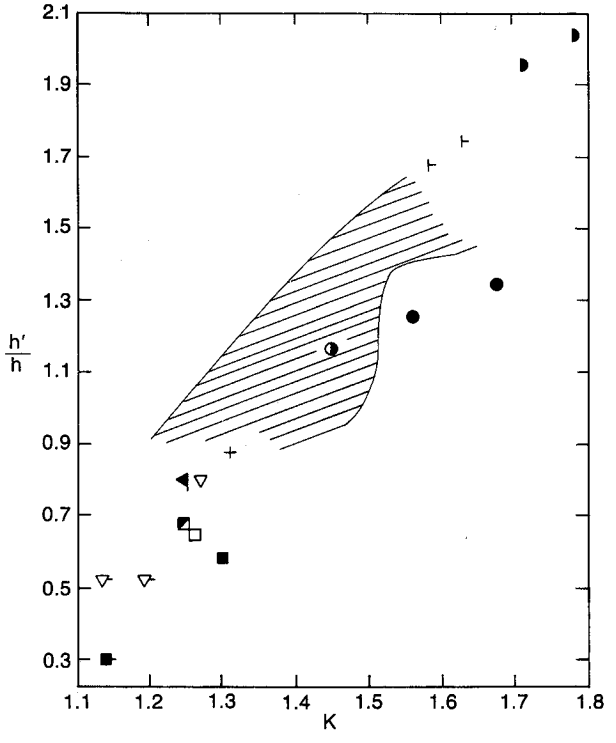

Fig. 7 Wake thickness, h'/h vs base pressure parameter K: □ $M = 0.6$, $Re \sim 1.4\times10^4$; ◪ $M = 0.6$, $Re \sim 4\times10^4$; ■ $M = 0.3$, $Re \sim 1.2\times10^3$; ■ $M = 0.3$, $Re \sim 1.2\times10^3$, with detached plate ($l = h$, $D = h$).

and due to Reynolds number dependence of the near-wake flow for the circular cylinder over the range 200–10^5.

Results from the present simulations are also compared with those from several laboratory experiments in Fig. 7, where the shaded area corresponds to a variety of body geometries and experimental (nearly incompressible) flow conditions given in Ref. 12, and the legend for the other experimental results is given in Table 2. Results from two simulations of the near wake in the absence of the interference plate correspond to the same physical conditions, with one case having twice the resolution in space and time as the other and, thus, corresponding to a higher Re regime. The results for the latter cases agree very well with each other and are associated with $Re \sim 1.4 \times 10^4$ and $Re \sim 4 \times 10^4$, respectively. A third such case corresponds to $M = 0.3$ and $Re \sim 1.2 \times 10^3$. The calculated results fall in the expected region of the figure for wake flows with blunt-based D-shaped models and are consistent with the overall similitude of the experimental data. In particular, the

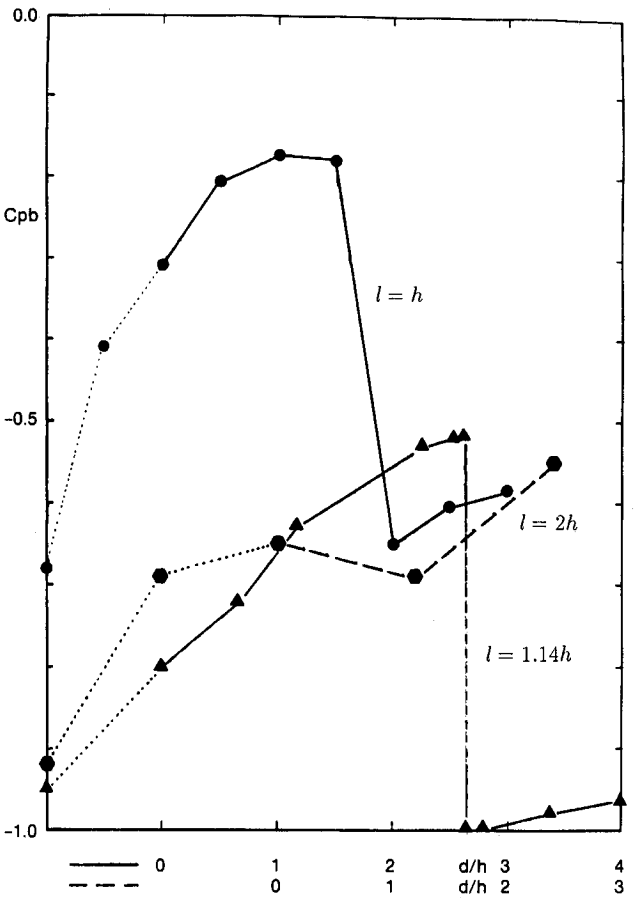

Fig. 8 Effect of attached plate. Simulations for $M = 0.3$ and $Re \sim 1.2\times10^3$: ● simulations; □ Bearman,[3] $Re = 1.45\times10^5$; ■ Bearman,[3] $Re = 2.45\times10^5$; ● Mansingh,[5] rectangular cylinder.

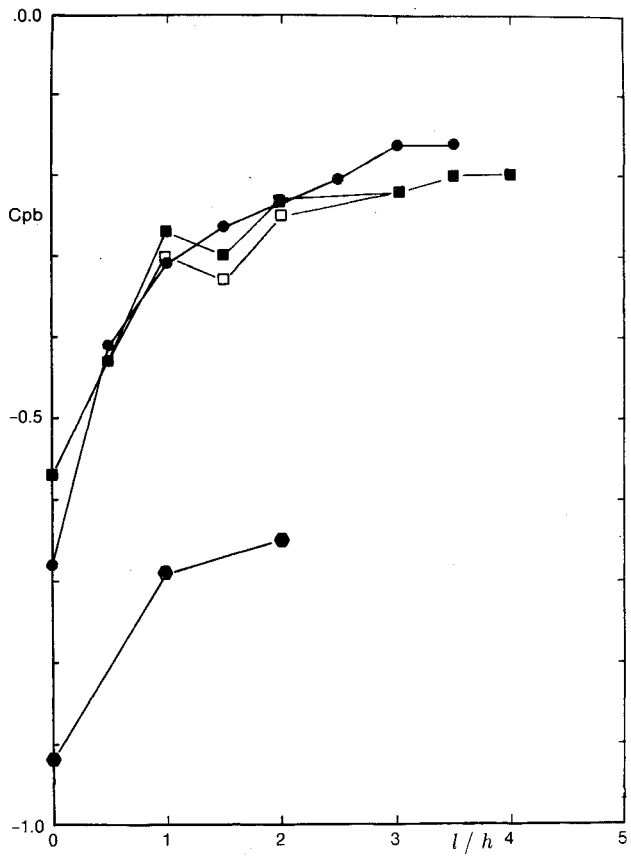

Fig. 9 Effect of detached plate ($l = h$). Simulations for $M = 0.3$ and $Re \sim 1.2\times10^3$: ● simulations, experiments; ▲ Roshko,[3] circular cylinder, diameter h, ($l = 1.14h$); ⬢ Mansingh,[5] ($l = 2h$).

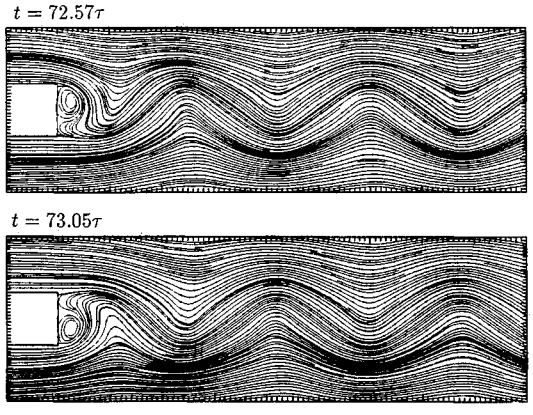

Fig. 10 Instantaneous streamlines for wake without interference. Simulations for $M = 0.3$ and $Re \sim 1.2\times10^3$. Time is scaled with the shedding period τ.

calculated base-pressure parameters K agree quite well with that in the (virtually incompressible) experiments with D-shaped bodies of Bearman ($Re = 1.45 \times 10^5$ to 2.45×10^5),[3] Blake ($Re = 10^5$),[15] and Simmons ($Re = 1.5 \times 10^4$),[14] which involved bluff-body flow configurations close to that studied in the present simulations. This observed agreement supports the expectation that the pressure drag is determined principally by the inviscid, large-scale vorticity dynamics. In the experiments by Bearman,[3] there was a significant contribution to the wake thickness due to the presence of thick turbulent boundary layers, whereas the simulations describe flows with laminar inflows and negligible effective boundary-layer thickness. This difference consistently explains the larger experimental values of the wake thickness h'/h in Fig. 7. The data points on the lower left corner of Fig. 7, having much smaller values of K and h', correspond to cases using interference plates, including results based on measurements with D-shaped laboratory models (attached plate)[3] and calculations for $M = 0.3$ and $Re \sim 1.2 \times 10^3$ (with a detached plate). A more detailed comparison of the latter data is given in Figs. 8 and 9.

Figure 8 shows calculated base-pressure coefficients C_{pb} obtained when the interference plate attached to the blunt-based body is included in the model. A vanishingly thin interference plate was used to modify the near-wake shedding pattern and, thus, the base pressure and body form drag. Results are shown for cases in which the length of the plate varied up to $l = 3.5h$. The base-pressure coefficient C_{pb} changes by a factor of up to 3 in this regime, in good quantitative agreement with the experimental results reported by Bearman,[3] especially with the data for larger Re.

Figure 9 shows results for the case in which an interference plate of fixed length $l = h$ had the separation between its leading edge and the base varied between 0 and $3h$. The dotted sections for the negative values of d/h correspond to cases with an attached plate of length smaller than the specified value of l. The base pressure increases beyond its low value in the attached case, attaining minimum drag when the leading edge is at $d \sim h$. This low-drag behavior is maintained to approximately a separation of $d \sim 1.5$–$2h$ where the drag increases again as the calculated C_{pb} drops sharply and both the base-pressure coefficient and the shedding frequency (see Table 1) approach the values for the case without interference.

The observed behavior of C_{pb} can be understood in terms of the way the vortex formation region is affected by the presence of the interference plate. The effects of the interference plate

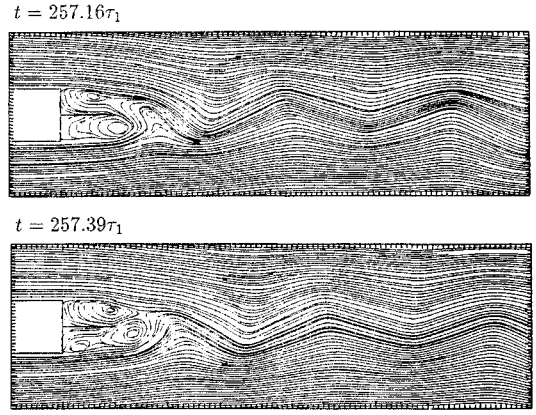

Fig. 11 Instantaneous streamlines for wake with attached interference plate ($l = h$). Simulations for $M = 0.3$ and $Re \sim 1.2\times10^3$. Time is scaled with the corresponding shedding period τ_1.

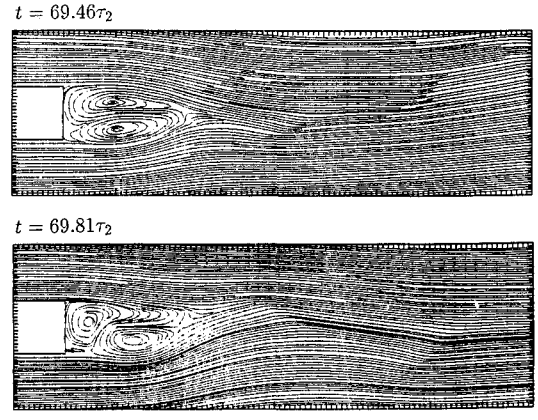

Fig. 12 Instantaneous streamlines for wake with detached interference plate ($l = h$, $d = h$). Simulations for $M = 0.3$ and $Re \sim 1.2\times10^3$. Time is scaled with the corresponding shedding period τ_2.

on the flow pattern are visualized through instantaneous (velocity-direction) streamline plots in Figs. 10–13 and through contours of u' in Fig. 14. Physically, the (attached) thin interference plate interrupts the shear layer crossflows as its length is increased (cf. Figs. 10 and 11), or for fixed interference plate length, as its leading edge is moved away from the base (Figs. 12 and 13). The attached interference plate of increasing length moves the region of intense shear layer interaction (vortex formation) downstream and increases the average base pressure as shown in Fig. 8.

The detached interference plate of fixed length also extends the vortex formation region (cf. Figs. 10 and 12), and thus increases the base pressure and reduces the drag. The greatest pressure-drag reduction is attained for a separation $d \sim h$. For $d = h$, the shedding frequency is quite smaller ($St = 0.11$) than that for the undisturbed case ($St = 0.24$) and the wake thickness is also significantly reduced to $h'/h = 0.3$ (Fig. 14). However, when the detached plate is moved still farther downstream, beyond the critical separation at which the sharp drop of the calculated C_{pb} occurs in Fig. 9, the shear layers are again free to interact as the shedding process is completed upstream of the plate's leading edge (Fig. 13) and the wake-interference effect is not significantly felt. This accounts for the rapid drop in base pressure observed in Fig. 9 for both the computations (between h–$1.5h$) and the experiments of Roshko[2] (between 2.5–$3h$). In the latter experiments, a circular cylinder and an interference plate of length $l = 1.14h$ were involved, and a qualitatively similar behavior was found for C_{pb} as a function of the separation d.

For qualitative comparison purposes, we have also included in Fig. 9 data from the experiments by Mansingh[5] with a rectangular cylinder ($L/h = 0.24$), which were conducted with a plate of fixed length $l = 2h$ (corresponding to the lower horizontal scale). Significantly lower pressure values were observed in the experiments by Roshko[2] and Mansingh[5] because of the distinctly greater bluffness of the rectangular and circular cylinders (separation angle at or greater than 90 deg) as compared to the D-section cylinders (separation angle at 0 deg). These experiments, together with the previous results discussed, effectively show the influence of passive wake control with interference plates on the vortex formation processes. Drag reduction by factors of up to 3 are possible.

The boundary-layer thickness at separation is effectively zero in the present simulations. The characteristics of the boundary layer and separated shear layers will play a role in microscale aspects of the near-wake vortex dynamics and the flow in the vortex formation region. Thus, for different bodies, the thickness of the separated shear layers and when they become turbulent are important considerations. It has generally been established that the near wake of a bluff body is a relatively large-size region of global instability[19] and that the vortex formation region represents a region of absolute instability.[1] Moreover, Chomaz et al.[20] have shown that the existence of a local absolute instability is a necessary, but not sufficient, condition for the presence of global-scale oscillations. Thus, the presence of the observed global instability does imply the presence of local absolute instability. The relation between local and global properties in the flow depends on the spatial slow-variation assumption, in this case in the downstream direction. This may be specified by a parameter ϵ, which can be represented, for example, by the ratio $\epsilon = \theta_s/h$, where θ_s is the initial shear-layer momentum thickness. It is crucial that ϵ be small in order to establish any possible analytic connection between local and global instability properties.[21] In the present simulations, the self-sustaining (global) instabilities were found to be intrinsic features of the flows investigated. Because of the essentially inviscid nature of the present simulations, the numerical solutions studied are characterized by having a boundary-layer thickness δ_s that is effectively very small (of the order of a computational cell) at separation. Since the momentum thickness θ_s is defined to be a fraction of δ_s, θ_s and the ratio ϵ can also be regarded as nearly zero, and thus, the results of the simulations are consistent with a local absolute/global instability scaling.

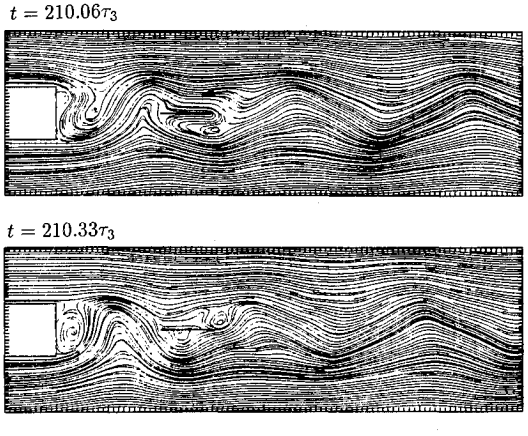

Fig. 13 Instantaneous streamlines for wake with detached interference plate ($l = h$, $d = 2h$). Simulations for $M = 0.3$ and $Re \sim 1.2\times10^3$. Time is scaled with the corresponding shedding period τ_3.

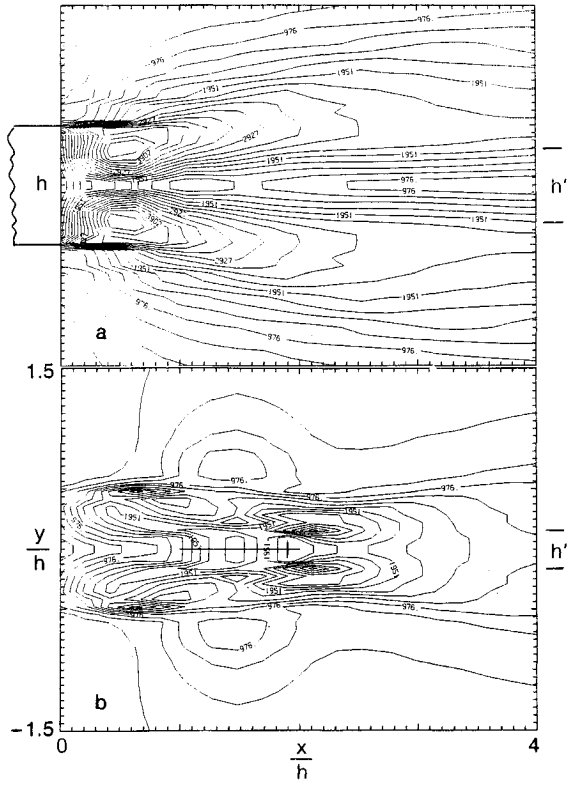

Fig. 14 Normalized rms velocity fluctuations u' ($\times10^4$): a) undisturbed wake; b) configuration with detached interference plate ($l = h$, $d = h$). Simulations for $M = 0.3$ and $Re \sim 1.2\times10^3$.

Summary and Conclusions

We have presented results from finite difference numerical simulations of a spatially evolving plane wake flow. The focus has been on the flow dynamics in the region of vortex formation and in the near wake as relevant for the control of base-pressure drag in nearly inviscid flow. We have shown the influence of passive wake control on base-pressure (or form) drag using a thin flow-aligned plate to interfere directly with the vortex formation process behind a long bluff body with rectangular cross section. The numerical experiments have examined the passive pressure-drag control in the plane wake as a function of the length of the interference plate attached to the base and in terms of the separation between the base and the fixed-length plate, in the detached case.

The numerical simulations reported here use an essentially inviscid formulation based on the Euler equations for compressible flow. The computations agree well with the base-pressure coefficients measured by Bearman,[3] Simmons,[14] and Blake et al.,[15] even though, as one example, the turbulent boundary-layer thickness at separation in Bearman's experiment was 50% of the D-section cylinder's base height. Good agreement was also found between the calculated and measured shedding frequencies. This agreement between the computations and the experiments in terms of macroscale wake properties is coupled to the relatively high Reynolds numbers in the experimental flows. Equally good agreement for the microscale wake properties is not so likely, particularly in the case of the two-dimensional simulation.

Acknowledgments

This work was supported by the Office of Naval Research, the Naval Research Laboratory, and the Defense Advanced Research Projects Agency Applied & Computational Mathematics Program. The calculations were performed at the computing facilities of the NAS at NASA Ames Research Center and at the LCP & FD Graphical and Array Processing System facility.

References

[1]Triantafyllou, G. S., Kupfer, K., and Bers, A., "Absolute Instabilities and Self-Sustained Oscillations in the Wakes of Circular Cylinders," *Phys. Rev. Lett.* Vol. 59, No. 17, 1987, pp. 1914–1917.

[2]Roshko, A., "On the Wake and Drag of Bluff-Bodies," *Journal of Aeronautical Sciences,* Vol. 22, 1955, pp. 124–132.

[3]Bearman, P. W., "Investigation of the Flow Behind a Two-Dimensional Model With a Blunt Trailing Edge and Fitted with Splitter Plates," *Journal of Fluid Mechanics,* Vol. 21, Pt. 2, 1965, pp. 241–255.

[4]Unal, M. F., and Rockwell, D., "On Vortex Formation From a Cylinder. Part 2. Control by Splitter-Plate Interference," *Journal of Fluid Mechanics,* Vol. 190, 1988, pp. 513–523.

[5]Mansingh, V., "Experimental Investigation of the Flow Behind a Rectangular Cylinder with a Wake Splitter Plate," Ph.D. Dissertation, Queen's Univ., Kingston, Ontario, Canada, 1986.

[6]Boris, J. P., Griffin, O. M., Baum, J. D., Gardner, J. H., Grinstein, F. F., Kailasanath, K., Oran, E. S., and Young, T. R., "Vortex Shedding and Base Pressure Behind a Wide Splitter Plate," *Flow Induced Vibration,* Vol. 154, edited M. K. Au-Yang, S. S., Chen, S. Kaneko, and R. Chilukuri, American Society of Mechanical Engineers, New York, 1989, pp. 147–154.

[7]Boris, J. P., Oran, E. S., Gardner, J. H., Grinstein, F. F., and Oswald, C. E., "Simulations of Spatially Evolving Compressible Turbulence," *9th International Conference on Numerical Methods in Fluid Mechanics,* edited by Soubbaramayer and J. P. Boujot, Springer-Verlag, New York, 1985, pp. 98–102.

[8]Grinstein, F. F., Guirguis, R. H., Dahlburg, J. P., and Oran, E. S., "Three-Dimensional Numerical Simulation of Compressible Spatially Evolving Shear Flows," *11th International Conference on Numerical Methods in Fluid Mechanics,* edited by D. L. Dwoyer, M. Y. Hussaini, and R. G. Voigt, Springer-Verlag, New York, 1989, pp. 283–287.

[9]Grinstein, F. F., Oran, E. S., and Boris, J. P., "Direct Numerical Simulation of Axisymmetric Jets," *AIAA Journal,* Vol. 25, 1987, pp. 92–98.

[10]Grinstein, F. F., Hussain, F., and Oran, E. S., "Vortex-Ring Dynamics in a Transitional Subsonic Free Jet. A Numerical Study," *Europ. J. Mech. B/Fluids,* Vol. 9, No. 6, 1990, pp. 499–525.

[11]Boris, J. P., Grinstein, F. F., Young, T. R., and Griffin, O. M., "Numerical Simulation of Passive Pressure-Drag Control in a Plane Wake," in preparation.

[12]Grinstein, F. F., and Guirguis, R. H., "Effective Viscosity in the Simulation of Spatially Evolving Shear Flows with Monotonic FCT Models," *Journal of Computational Physics* (submitted for publication).

[13]Griffin, O. M., "Universal Similarity in the Wakes of Stationary and Vibrating Bluff Structures," *Journal of Fluids Engineering,* Vol. 103, 1981, pp. 52–58.

[14]Simmons, J. E. L., "Similarities Between Two-Dimensional and Axisymmetric Vortex Wakes," *The Aeronautical Quarterly,* Vol. 26, No. 1, 1977, pp. 15–20.

[15]Blake, W. K., Maga, L. J., and Finkelstein, G., "Hydroelastic Variables Influencing Propeller and Hydrofoil Singing," *Noise and Fluids Engineering,* American Society of Mechanical Engineers, New York, 1977, pp. 191–199.

[16]Heinemann, H. J., Lawaczeck, O., and Butefisch, K. A., "Karman Vortices and Their Frequency Determination in the Wakes of Profiles in the Sub- and Transonic Regime," *Symposium Transsonicum II Gottingen,* Sept. 1975, Springer-Verlag 1976, pp. 75–82.

[17]Armstrong, B. J., Barnes, F. H., and Grant, I., "A Comparison of the Structure Behind a Circular Cylinder in a Steady Flow With That in a Perturbed Flow," *Phys. Fluids,* Vol. 30, 1987, pp. 19–26.

[18]Barbi, C., Favier, D. P., Maresca, C. A., and Telionis, D. P., "Vortex Shedding and Lock-On of a Circular Cylinder in Oscillating Flow," *Journal of Fluid Mechanics,* Vol. 170, 1986, pp. 527–544.

[19]Huerre, P., and Monkewitz, P. A., "Absolute and Convective Instabilities in Free Shear Layers," *Journal of Fluid Mechanics,* Vol. 159, 1985, pp. 151–168.

[20]Chomaz, J. M., Huerre, P., and Redekopp, L. G., "Bifurcations to Local and Global Modes in Spatially Developing Flows," *Physical Review Letters,* Vol. 60, No. 1, 1988, pp. 25–28.

[21]Huerre, P., and Monkewitz, P. A., "Local and Global Instabilities in Spatially Developing Flows," *Annual Review of Fluid Mechanics,* Vol. 22, 1990, pp. 473–537.